

**Acoustics'08
Paris**
June 29-July 4, 2008

www.acoustics08-paris.org

Accurate ultrasonic measurement of two-dimensional displacement of heart wall motion for estimation of myocardial regional strain rate

Yasunori Honjo, Hideyuki Hasegawa and Hiroshi Kanai

Department of Electronic Engineering, Graduate School of Engineering, Tohoku University,
6-6-05 Aramaki-aza-Aoba, Aoba-ku, 980-8579 Sendai, Japan
honjo@us.ecei.tohoku.ac.jp

Methods for imaging of strain rate in the heart wall are useful for quantitative evaluation of regional heart function. We developed a method which can accurately measure the heart wall motion along an ultrasonic beam based on phase changes in RF echoes. However, there are some components in the wall motion which are not along each ultrasonic beam. Therefore, the measurement of motion in the direction perpendicular (lateral) to the beam has been required in addition to that in the axial direction. However some unsolved problems remain in estimation of the distribution of lateral motion of the wall. In this study, two-dimensional displacement was estimated by 2-D cross-correlation between RF echoes. Important parameters, the sizes of a region-of-interest and search region, which determine tracking accuracy, were adaptively optimized by referring to instantaneous wall velocities, in the respective cardiac phases. The correlation coefficient between the lateral displacement estimated by the 2-D tracking with optimized parameters in longitudinal-axis view and in apical view (corresponding to lateral displacement in longitudinal-axis view) separately and accurately estimated by the 1-D phase-based method was 0.93. These results show possibility of this method for accurate measurement of two-dimensional heart motion to assess the regional myocardial strain rate.

1 Introduction

The most practical modality for estimation of the myocardial function used in noninvasive clinical medicine is B-mode and M-mode imaging using ultrasonic diagnostic equipment. However, the qualitative diagnosis based on B-mode and M-mode imaging depends on the operator's experience, and so on. Methods for imaging of 1-D and 2-D strain rate in the heart wall are useful techniques for the quantitative evaluation of regional heart function [1, 2, 3, 4]. We developed a method (1-D phase-sensitive method) which can accurately measure the heart wall motion along an ultrasonic beam based on phase changes in RF echoes [5]. However, there are some components in the wall motion which are not along each ultrasonic beam. Therefore, the measurement of motion in the direction perpendicular (lateral) to the ultrasonic beam has been required in addition to that in the axial direction. However, some unsolved problems remain in 2-D tracking of the heart wall.

2 Materials and Methods

2.1 2-D cross-correlation function

Heart wall motion has been estimated using some algorithms, speckle tracking [6, 7, 8] (based on cross-correlation, normalized cross-correlation, sum of absolute differences, sum of squared differences), optical flow [9] and so on. The algorithm based on the correlation coefficient between ultrasonic RF echoes is one of the most available methods to estimate the heart motion [10]. In this study, 2-D displacement was estimated by 2-D cross-correlation between RF echoes. The correlation coefficient $r_n(\Delta N, \Delta l, \Delta d)$ at the axial and lateral shifts, Δd and Δl , is calculated from RF signal $rf_n(l, d)$ at depth d and beam position l in the n -th frame as follows:

$$r_n(\Delta N, \Delta l, \Delta d) = \frac{1}{A} \sum_{i=l-L/2}^{l+L/2} \sum_{j=d-D/2}^{d+D/2} \{rf_n(i, j) \cdot rf_{n+\Delta N}(i+\Delta l, j+\Delta d)\}, \quad (1)$$

$$(A = (L+1)(D+1)\sigma_{n,l,d}\sigma_{n+\Delta N,l+\Delta l,d+\Delta d})$$

where $\sigma_{n,l,d}$ is the standard deviation of the RF signal $rf_n(l, d)$ in a $((L+1) \times (D+1))$ region of interest. RF signals in the ROI in the n -th frame are compared with those in the $(n+\Delta N)$ -th frame. The ROI in the $(n+\Delta N)$ -th frame is shifted by Δd and Δl in the axial and lateral directions relative to those in the n -th frame.

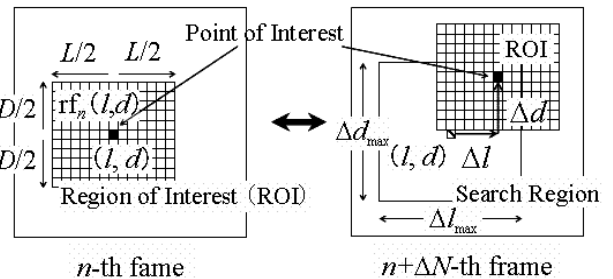


Fig.1 Calculation of cross-correlation function between RF signals in n -th frame and $n+\Delta N$ frame.

2.2 1-D phase-sensitive method

To successfully track the heart motion using 2-D cross-correlation function, the important parameters, the sizes of a region-of-interest ($L \times D$) and search region ($\Delta l_{max} \times \Delta d_{max}$), which determine tracking accuracy, were adaptively optimized by referring to instantaneous wall velocities, in the respective cardiac phases.

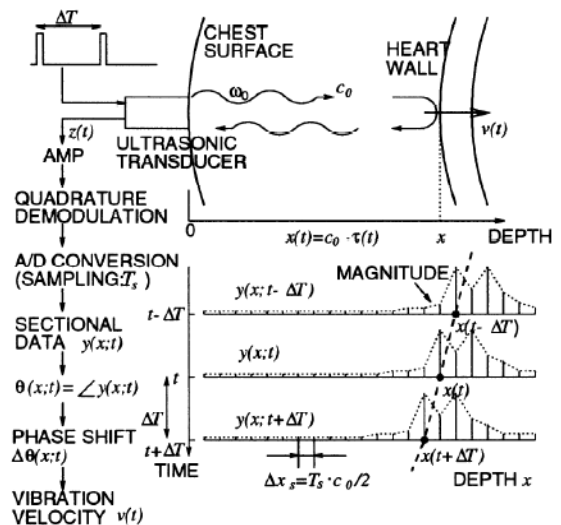


Fig. 2 Estimation of the velocities in the heart wall using the 1-D phase-sensitive method [5].

In this study, the regional displacement of the heart wall is estimated by a 1-D phase-sensitive method which was

developed by our group to optimize the sizes of an ROI and search region. RF pulses with angular frequency $\omega_0 = 2\pi f_0$ are transmitted at a time interval ΔT from a sector-type probe placed on the chest surface as shown in Fig. 2.

The ultrasonic pulse is reflected by the heart wall. Then, the received signal, $z(t)$, is amplified and the quadrature demodulation is applied to the received signal. The received RF signal is A/D converted at a sampling period of T_s and then demodulated into the complex signals $\{y(x; n)\}$, where x denotes the distance from the sector probe.

The phase change $\gamma_n(\delta_x)$, can be obtained from the complex correlation function between $y(x; n)$ and $y(x + \delta_x; n + \Delta N)$, defined as follows:

$$\hat{\gamma}_n(\delta_x) = \frac{\sum_{x \in R} y^*(x; n) \cdot y(x + \delta_x; n + \Delta N)}{\left| \sum_{x \in R} y^*(x; n) \cdot y(x + \delta_x; n + \Delta N) \right|} \quad (2)$$

The average velocity during period ΔT is estimated using phase of $\hat{\gamma}_n(\delta_x)$ as follows:

$$\hat{v}(x; n) = c_o \frac{\angle \hat{\gamma}_n(\delta_x)}{2\omega_0 \Delta T}, \quad (3)$$

where $\angle \hat{\gamma}_n(\delta_x)$ denotes the phase value in radian of $\hat{\gamma}_n(\delta_x)$. The heart wall position in the next frame is obtained by multiplying the velocity $\hat{v}(x; n)$ estimated by eq. (3) by period ΔT .

$$\hat{x}(n+1) = \hat{x}(n) + \hat{v}(x; n) \cdot \Delta T. \quad (4)$$

2.3 Acquisition of RF signals for 2-D tracking

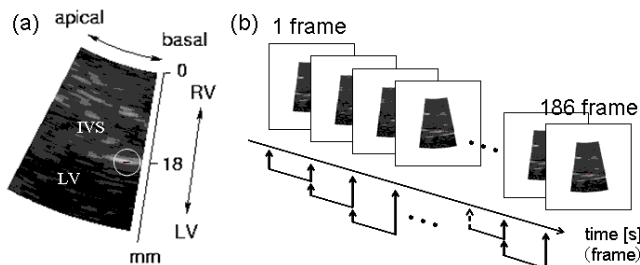


Fig.3 (a) Acquired cross-sectional image of heart wall. (b) calculation of cross-correlation function between frames.

As illustrated in Fig. 3(a), the interventricular septum (IVS) is measured and the ultrasonic beam scanned densely so that the IVS can be measured at a high spatial resolution. RF data are acquired using a 3.75-MHz sector-type probe of ultrasonic diagnostic equipment (Aloka SSD-6500). The sampling frequency of the RF signal was 15 MHz. The frame rate and angular interval of beams are 260 Hz and 0.75 degree, respectively.

2.4 Acquisition of RF signals for 1-D estimation

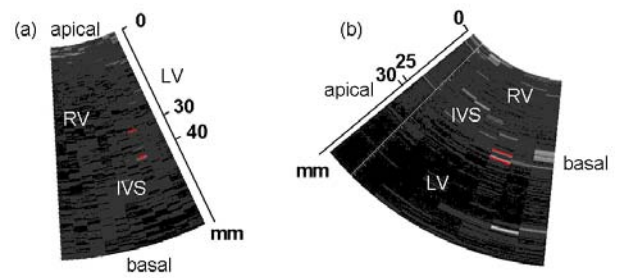


Fig. 4 B-mode cross-sectional imaging of heart in the apical four-chamber longitudinal-axis view (a) and interventricular septum longitudinal-axis view (b).

As illustrated in Fig. 4, the interventricular septum (IVS) was measured in the apical four-chamber longitudinal-axis view and interventricular septum longitudinal-axis view with the ultrasonic beam scanned sparsely. RF data were acquired using a 3.75-MHz sector-type probe of ultrasonic diagnostic equipment (Aloka SSD-6500). The sampling frequency of the RF signal was 15 MHz. The frame rate and angular interval of beams were 526 Hz or 522 Hz and 2.25 degree, respectively.

2.5 Estimation of displacement along beam direction

As illustrated in Figs. 5(1-a) and 5(2-a), the lateral displacement of the interventricular septum in the longitudinal-axis view of the left ventricle corresponds approximately to the axial displacement in the apical view obtained by 1-D estimator. Therefore, the important parameters, sizes of a region of interest and a region for correlation search, which determine tracking accuracy, were adaptively optimized by referring to the axial displacement in the apical view as the true lateral displacement in the longitudinal-axis view. Figures 5(1-b) and 5(2-b) show M-mode images in the apical view and longitudinal-axis view, respectively. Both displacements along beam directions in the longitudinal-axis and apical views were calculated by means of the 1-D phase-sensitive method.

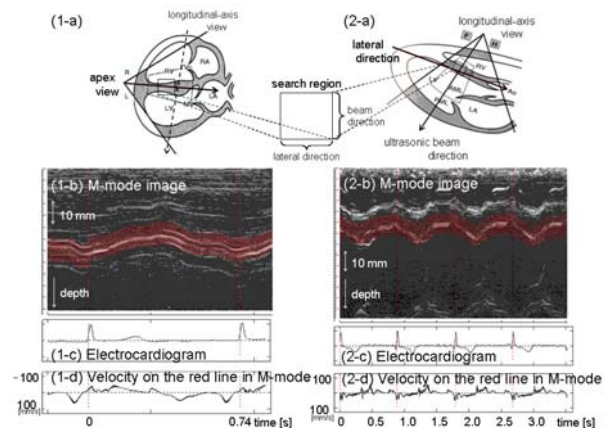


Fig. 5 Results obtained in apical four-chamber view (1) and interventricular septum (2). (a) Illustrations cross-sectional images of heart wall. (b) M-mode image and displacements shown by red lines. (c) Electrocardiograms. (d) Velocities on the red lines in M-mode image.

3 Estimation of determined parameters

3.1 Determination of optimum size of search region

The displacements Y_n and X_n along beam direction in the apical (1) and longitudinal-axis (2) views obtained by the 1-D phase-sensitive method ($n = 0, 1, 2, \dots$) were calculated from displacements y_n and x_n between two consecutive frames as follows:

$$X_n = \sum_{i=1}^n x_i, \quad Y_n = \sum_{i=1}^n y_i. \quad (5)$$

The displacements $Z_{x,m}$ and $Z_{y,m}$ in the axial and lateral directions in the longitudinal-axis view obtained by 2-D tracking ($m = 0, 1, 2, \dots$) were calculated from displacements $z_{x,m}$ and $z_{y,m}$ between two consecutive frames as follows:

$$Z_{xm} = \sum_{j=1}^m z_{xj}, \quad Z_{ym} = \sum_{j=1}^m z_{yj}. \quad (6)$$

Frame rates were different among the measurements. Frame rates f_A and f_L in the measurement of axial displacements in the apical and longitudinal views are expressed by the numbers, m_A , m_L , and n , of measured frames in the apical, longitudinal-axis, and longitudinal-axis (for 2-D tracking) views as follows:

$$f_A \times m_A = f_Z \times n, \quad f_L \times m_L = f_Z \times n, \quad (7)$$

where f_Z is the frame rate in the measurement in the longitudinal-axis view for 2-D tracking. Then, τ_A and τ_L denotes proportion of f_A to f_Z ($= f_A / f_Z$) and that of f_L to f_Z ($= f_L / f_Z$). The displacements $z_{x,m}$ and $z_{y,m}$ between the m -th and $(m+1)$ -th frames by 2-D tracking are represented by x_n and y_n , which are obtained by the 1-D phase-sensitive method as follows:

$$Z_{x,m} = \sum_{k=0}^{\tau'_A-1} x_{\tau'_A \cdot m+k}, \quad Z_{y,m} = \sum_{k=0}^{\tau'_L-1} y_{\tau'_L \cdot m+k}. \quad (8)$$

where τ'_A and τ'_L are integers which are closest to τ_A and τ_L , respectively. The size of a search region is determined by referring to displacements x_i and y_i between two frames which are obtained by the 1-D phase-sensitive method. The search region should be larger than the displacement between two frames. However, there may be several regions in the post frame which have echo patterns similar to that in the region of interest in the previous frame when the size of the search region is too large. The velocity of heart motion is different phase by phase in one cardiac cycle. In isovolumic, relaxation, and atrial systole phases, the wall velocity is high. On the other hand, that is low in ejection and filling phases [11]. Therefore, in this study, sizes of search regions were adaptively determined by $z_{x,m} \times z_{y,m}$.

3.2 Determination of optimum size of region-of-interest

In terms of the size of an ROI, when the size of a region-of-interest is set to be small, fluctuation of estimated displacement is large [12]. On the other hand, when the size of a region-of-interest is set to be large, the echo pattern in a region-of-interest is more unique and the displacement estimation is less susceptible to noise. However, the spatial resolution degrades at the same time [7]. There is a trade-off between its size and accuracy of the estimate. Therefore, the optimum size of a region-of-interest in 2-D tracking was investigated. Regions of interest with different sizes ($l \times d$) = ((1.5 ~ 7.5 degree) \times (0.1 ~ 3.1 mm)) were examined to determine the optimum size. The two dimensional displacement of a region of interest in the interventricular septum was estimated by two dimensional cross-correlation function with regions-of-interest with different sizes and the search region whose size was determined by displacement between two consecutive frames obtained by 1-D method. The reliabilities of the axial and lateral displacements obtained by 2-D tracking were evaluated using correlation coefficients between displacements estimated by the 2-D method and corresponding displacements obtained by the 1-D method in two different views as follows:

$$c_{zX} = \frac{1}{n_z \sigma_{z_x} \sigma_{X_n}} \sum_{n=1}^{n_z} z_{x,n} \cdot X_n, \quad (9)$$

$$c_{zY} = \frac{1}{n_z \sigma_{z_x} \sigma_{Y_n}} \sum_{n=1}^{n_z} z_{x,n} \cdot Y_n, \quad (10)$$

In Eq. (9), c_{zX} is the cross-correlation coefficient between the lateral displacement estimated by the 2-D method and the axial displacement in the apical four-chamber view as reference, and, c_{zY} is that between the axial displacement estimated by the 2-D method and the axial displacement in the IVS longitudinal-axis view, respectively.

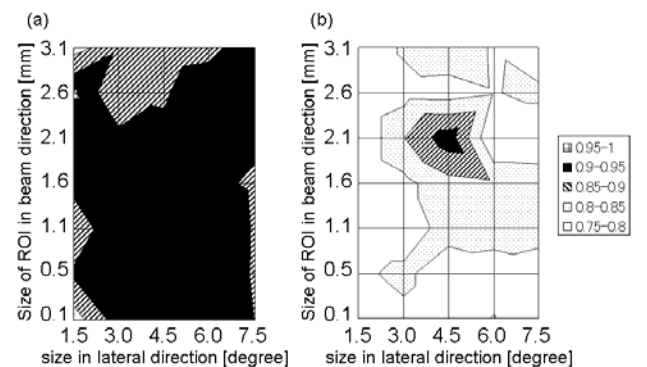


Fig. 6 Cross-correlation coefficients (a) between the axial displacement estimated by the 2-D method and reference. (b) between the lateral displacement estimated by the 2-D method and reference.

As illustrated in Fig. 6, these contours show the cross-correlation coefficient which was averaged for 4 cardiac cycle. Fig. 6 (a) shows that the correlation coefficient c_{zY} . Correlation coefficient c_{zY} is totally high (0.9~0.95). This result shows the axial displacement can be estimated accurately by 2-D tracking with any size of a region of interest.

On the other hand, Fig. 6(b) shows the correlation coefficient c_{zX} . The contour shows different tendency compared with that in Fig. 6(a). The distribution of correlation coefficient c_{zX} shows a dominant peak at a size of a region of interest of (4.5 deg×2.1 mm). Therefore, in this study, the size of a region-of-interest are determined to be (4.5 deg×2.1 mm).

4 Basic experiment using a phantom

4.1 Experimental system

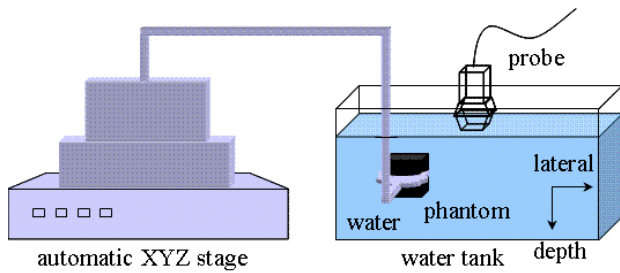


Fig. 7 Schematic of system for basic experiments.

As illustrated in Fig. 7, accuracy of 2-D tracking using determined parameters, sizes of search region and region-of-interest, was evaluated by basic experiments. A phantom was silicon rubber whose thickness is nearly same as that of IVS ((length×width×thickness) = (50×60×15) mm). The motion velocity of the phantom was controlled by an automatic XYZ stage. The evaluation was conducted for two types of motion, 1-D motion in the lateral direction and 2-D motion including axial motion.

4.2 Measurement of lateral motion

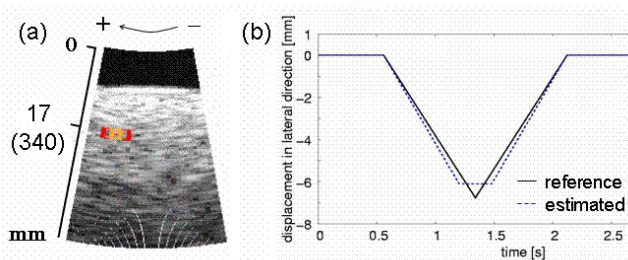


Fig. 8 (a) B-mode cross-sectional image of the phantom.
(b) Estimated lateral displacement.

At first, the phantom was moved in only the lateral direction by the automatic XYZ stage and its velocity was set at 8 mm/s. The typical cross-sectional image of the silicon rubber is shown in Fig. 8(a). The frame rate was 163 Hz, the frame interval for calculating correlation function was 20 frames (0.12 ms), and the beam angle between neighbor beams was 0.75 degree. The determined parameters, sizes of search region and region of interest, were set to be constant, and a region of interest of (4.5 deg×2.1 mm) in size was manually assigned in the first frame. The lateral motion at a point (in Fig. 8, (beam, depth) = (20th, 17 mm)) was tracked by 2-D cross-correlation function. Figure 8(b) shows the estimated displacement in the lateral direction and reference. Both displacements were very similar but the transition of

motion from right side to left side cannot be measured accurately, due to a large interval of frame.

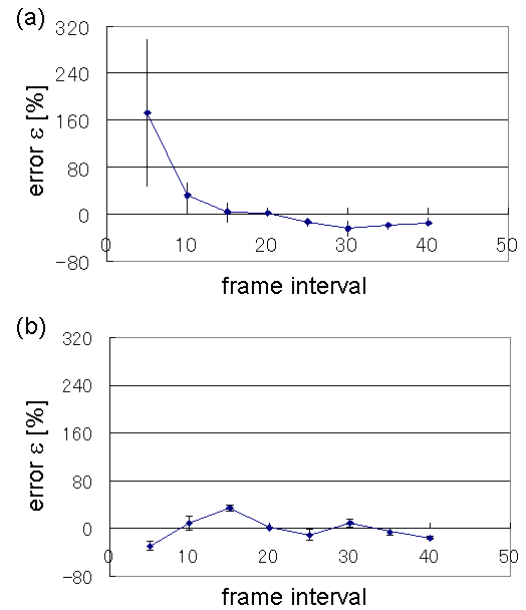


Fig. 9 Error of the estimated lateral displacements during motion (a) from left to right and (b) from right to left.

Figure 9(a) and 9(b) show errors in the lateral displacement during motions from left to right and from right to left, respectively, evaluated at different frame intervals for calculating the 2-D correlation function. The lateral displacements at 6 different positions in the phantom were estimated, and plots and vertical bars show means and standard deviations with respect to these 6 positions. The error was defined by the ratio of the mean difference $E_i[|v_i - v_{true}|]$ between the estimated velocity v_i (i : frame number) and the true velocity v_{true} of 8 mm/s during 20 frames to the true velocity v_{true} as follows:

$$\varepsilon_{error} = \frac{E_i[|v_i - v_{true}|]}{v_{true}} \times 100, \quad (11)$$

where $E_i[|]$ is the averaging operation. Velocity v_i was obtained from displacement z_{xi} between two frames. As illustrated in Fig. 9, when the interval was set 20 frames, the error ε of estimated displacement was the smallest.

4.3 Measurement of 2-D motion

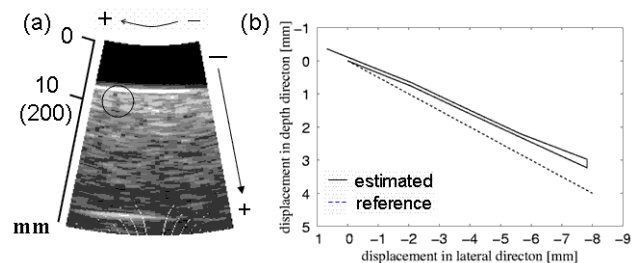


Fig. 10 (a) B-mode cross-sectional image of the phantom.
(b) Estimated 2-D displacement.

The phantom was moved 2-dimensionally. Lateral and axial velocities were set at 8 mm/s and 4 mm/s, respectively. As in the previous section, the parameters for calculating the correlation function were set to be constant by referring to the determined optimum values. A region of interest with a

size of (4.5 deg×2.1 mm) was manually assigned in the first frame. The lateral and axial motion at a point (in Fig. 10, (beam, depth) = (20th, 10 mm)) was tracked by 2-D cross-correlation function. As shown in Fig. 10 (b), the displacement estimated by 2-D tracking was in good agreement with the true value.

5 In vivo Experiment

5.1 Experimental results

Motion of a region in the IVS (beam, depth) = (3th, 18 mm) was estimated by 2-D tracking. As illustrated in Fig.3(b), the interval of frames was set at 1 and the 2-D cross-correlation function was calculated between two consecutive frames. As illustrated in Fig. 11(a) and 11(b), sizes of search regions were adaptively determined by referring to instantaneous heart wall velocity and displacement ($z_{x,m} \times z_{y,m}$) during a cardiac cycle. Figure 11 (a) is the velocity of the IVS in the axial direction obtained by 1-D phase-sensitive method and Fig. 11(b) is the velocity of the IVS in axial direction in the apical four-chamber view. The size of the region of interest was set at the determined optimum size (lateral × axial) = (4.5 deg×2.1 mm). Figure 11(c) shows the two-dimensional IVS motion obtained by the 2-D correlation function. Figure 11(c) shows that the interventricular septum moved to the apical side during cardiac systole and then, it began to return to the original position during diastole.

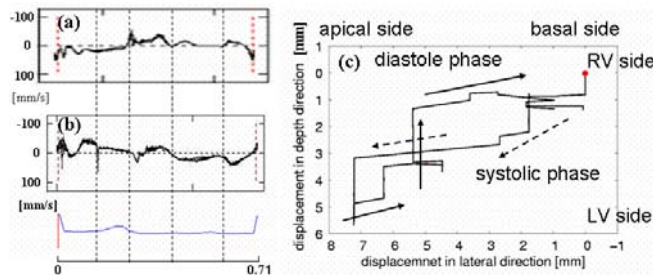


Fig. 11 (a) Velocity of the heart wall in depth direction. (b) Velocity in lateral direction. (c) 2-D estimated displacement.

5 Conclusion

The parameters, size of search region and region of interest, in 2-D estimation were determined to be optimal by referring to the separate measurements by the 1-D method in the different views. *In vivo* experimental results of 2-D tracking of the heart wall show possibility of this method for accurate measurement of two-dimensional heart motion for assessment of the regional myocardial strain rate.

References

[1] J. D'hooge, B. Bijnens, J. Thoen, F. van de Werf, G. R. Sutherland and P. Suetens, "Echocardiographic Strain and Strain-Rate Imaging: A New Tool to Study Regional Myocardial Function", IEEE Trans. Med. Imaging, Vol. 21, No. 9, pp. 1022-1030 (2002).

[2] J. D'hooge, E. Konofagou, F. Jamal, A. Heimdal, L. Barrios, B. Bijnens, J. Thoen, F. van de Werf, G. R.

Sutherland and P. Suetens, "Two-Dimensional Ultrasonic Strain Rate Measurement of the Human Heart *In Vivo*", IEEE Trans. UFFC., Vol. 49, No. 2, pp. 281-286 (2002).

- [3] M. Kowalski, T. Kukulski, F. Jamal, J. D'hooge, F. Weidemann, F. Rademakers, B. Bijnens, L. Hatle and G. R. Sutherland, "Can Natural Strain and Strain Rate Quantify Regional Myocardial Deformation? A Study in Healthy Subjects", Ultrasound in Med. & Biol., Vol. 27, No. 8, pp. 1087-1097 (2001).
- [4] S. Langeland, P. F. Wouters, Piet Claus, H. Alex Leather, Bart Bijnens, George R. Sutherland, Frank E. Rademakers and Jan D'hooge, "Experimental Assessment of A New Research Tool for the Estimation of Two-Dimensional Myocardial Strain", Ultrasound Med. Biol., Vol. 32, No. 10, pp. 1509-1513 (2006).
- [5] Hiroshi Kanai, Michie Sato, Yoshiro Koiwa and Noriyoshi Chubachi, "Transcutaneous Measurement and Spectrum Analysis of Heart Wall Vibrations", IEEE Trans. UFFC., Vol. 43, No. 5, pp. 791-810 (1996).
- [6] S. Langeland, J. D'hooge, H. Torp, B. Bijnens and P. Suetens, "Comparison of Time-Domain Displacement Estimators for Two-Dimensional RF Tracking", Ultrasound Med. Biol., Vol. 29, No. 8, pp. 1177-1186 (2003).
- [7] L. N. Bohs, B.J. Geiman, M.E. Anderson, S. C. Gebhart, G. E. Trahey, "Speckle Tracking for Multi-Dimensional Flow Estimation", Ultrasonics, Vol. 38, pp. 369-375 (2000).
- [8] S. Langeland, J. D'hooge, T. Claessens, P. Claus, P. Verdonck, P. Suetens, George R. Sutherland and Bart Bijnens, "RF-based Two-Dimensional Cardiac Strain Estimation: A Validation Study in a Tissue-Mimicking Phantom", IEEE. Trans. UFFC., Vol. 51, No. 11, pp. 1537-1546 (2004).
- [9] V. Behar, D. Adam, P. Lysyansky and Z. Friedman, "Improving Motion Estimation by Accounting for Local Image Distortion", Ultrasonics, Vol. 43, pp. 57-65 (2004).
- [10] I. Cespedes, Y. Huang, J. Ophir and S. Spratt, "Methods for Estimation of Subsample Time Delays of Digitized Echo Signals", Ultrasonic Imaging, Vol. 17, pp. 142-171 (1995).
- [11] B. Lind, J. Nowak, J. Dorph, J. van der Linden and L.-A. Brondin, "Analysis of Temporal Requirements for Myocardial Tissue Velocity Imaging", Eur J Echocardiography Vol.3, pp. 214-219 (2002).
- [12] D. Rappaport, D. Adam, P. Lysyansky and S. Riesner, "Assessment of Myocardial Regional Strain and Strain Rate by Tissue Tracking in B-mode Echocardiograms", Ultrasound Med. Biol., Vol. 32, No. 8, pp. 1181-1192 (2006).